Halogenated imidazo[1,5-a]pyridines: chemical structure and optical properties of a promising luminescent scaffold

Halogenated imidazo[1,5-a]pyridines: chemical structure and optical properties of a promising luminescent scaffold

G. Volpi, C. Garino*, E. Priola, C. Magistris, M.R. Chierotti, C. Barolo

Dipartimento di Chimica, NIS Interdepartmental Centre, Università di Torino, Via Pietro Giuria 7, 10125, Torino, Italy. *Fax: +39 011 670 7855; Tel: +39 011 670 7943; E-mail: claudio.garino@unito.it*

Keywords: imidazo[1,5-a]pyridine, luminescence, fluorescence, large Stokes shift, halogen bond

Abstract

A series of halogenated imidazo[1,5-a]pyridines was prepared and their structural and optical properties investigated. The products were characterized by spectroscopic techniques and their optical properties discussed in relation to their chemical structure. We were able to triplicate the luminescence quantum yields (φ) in solution for three different imidazo[1,5-a]pyridine derivatives, depending on the halogen nature of the substituent on the imidazo[1,5-a]pyridine moiety. The effect of the halogen and of the geometrical and chemical characteristics of the molecular skeleton on the crystal packing was studied in the solid state by single crystal X-ray diffraction. At the same time, the possible presence of halogen bonds was evaluated through solid-state NMR analysis.

1. Introduction

Heteroaromatic scaffolds, in which the nitrogen atoms are positioned at ring-fusion sites, represent an essential category of compounds due to their promising photophysical and biological properties [1]. In particular, substituted imidazo[1,5-a]pyridines are well known for their pharmaceutical and biological activity [2–6], as ligands for transition metal ions and as organic emitters with large Stokes shifts [7–9].

In the last few years, increasing attention has been paid to the imidazo[1,5-a]pyridine nucleus. Derivatives of the imidazo[1,5-a]pyridine nucleus have been applied in a variety of technological applications [10–12], including organic thin-layer field effect transistors (OFETs), UV absorption and organic light-emitting diodes (OLEDs) [13–15], owing to their optical tunability, inexpensiveness and the practicable scale-up of the synthesis towards industrial application.

Concerning the synthetic approach, several methods have been recently reported to promote this useful heterocyclization, involving the use of different catalysts, solvents and reagents [16–26]. On the other hand, synthetic strategies that enable the preparation of imidazo[1,5-a] pyridine derivatives containing useful pendant functional groups would be particularly attractive because they could be employed to provide new products with modified π-conjugated systems and fine-tuned optical and physical properties. To this end, halogenated imidazo[1,5-a]pyridines represent the perfect candidates for successive well-known cross-coupling reactions, as previously reported by Shibahara and coworkers [27,28].

Although the literature reports on deep design, intense synthetic effort and accurate optical and structural characterizations of these derivatives, a systematic investigation is still needed, in order to understand the relations between chemical structure (or chemical substituents) and photophysical behaviour. For this purpose, we have prepared, characterized and studied two series of 3-substituted and 1,3-disubstituted imidazo[1,5-a]pyridines (Scheme 1) of which two are new compounds, **5** and **9**, while the others were previously reported in literature. The modification of the optical properties in relation to the halogenated substituent groups on the imidazo[1,5-a]-pyridine scaffold was evaluated.

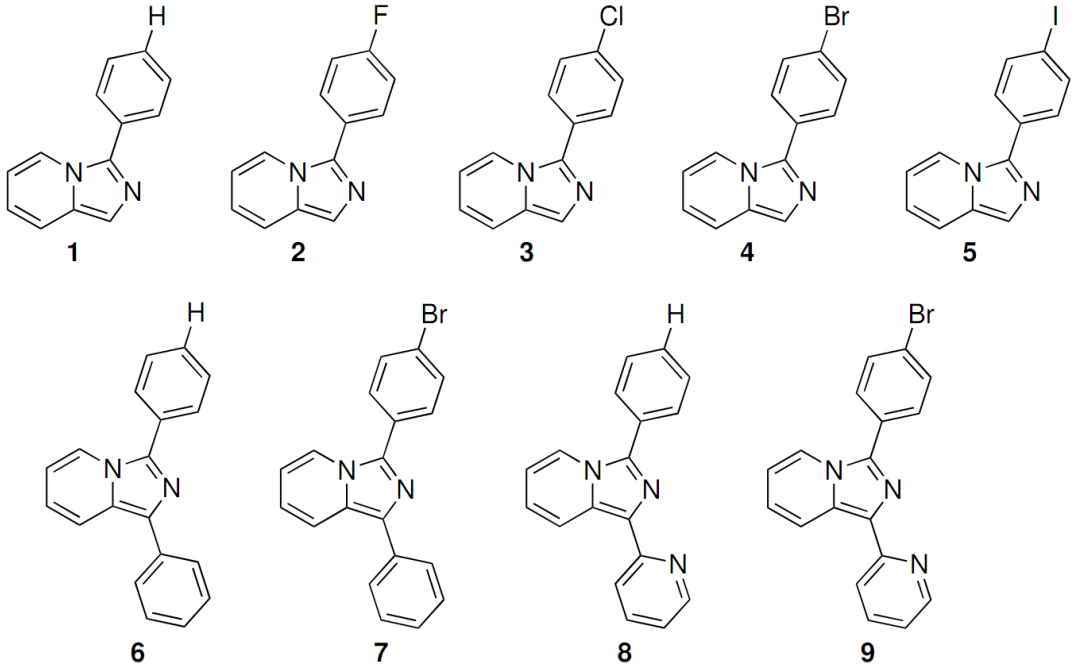

Scheme 1. Structures of studied imidazo[1,5-a]pyridines **1**–**9**.

2. Results and discussion

2.1. Synthesis

Compound **1**–**9** are based on the fluorescent imidazo[1,5-a]pyridine nucleus. They were obtained using previously reported one-potcyclizations in mild conditions [29,30]. Compounds **1**–**5** were prepared by condensation of 2-picolylamine with different 4-substituted-carboxylic acids in n-butylacetate and T3P (Propylphosphonic anhydride solution) in previously reported conditions [31,32]. Notably, the use of this synthetic approach, combined with microwave irradiation, resulted in a significant increase of the reaction yields (from 60 to over 90%), making this microwave based synthetic approach useful for a systematic screening of a large number of different intermediates.
Compounds **6**–**9** were obtained by condensation of phenyl(pyridin-2-yl) ketone (**6**, **7**) or di(pyridin-2-yl)ketone (**8**, **9**) with different 4-substituted-benzaldehydes in acetic acid under previously reported conditions [33].

2.2 Structural analysis

Compounds **4**, **5**, **6**, **7** and **9** were crystallized by slow evaporation of acetone (**2**, **4**), ethanol (**5**) and acetonitrile (**7**, **9**), and their crystals investigated by means of single crystal X-ray diffraction. The differences in their crystal packing were analysed in terms of: 1) the possible occurrence of halogen bond and the effect of the substitution of the pending halogen; 2) single (position 1) or double (position 1,3) substitution on the imidazo[1,5-a]pyridines skeleton; 3) the effect of the presence of an additional pyridinic nitrogen. The first effect can be evaluated comparing the structures of **6** and **7**, which differ for the presence/absence of the halogen, or considering **4** and **5**, which differ for a bromine instead of an iodine atom. Both substitutions can drastically affect the tendency of the molecule toward X···N halogen bond formation [34].
The differences between the crystal packing of the bromine and the iodine substituted molecules are completely negligible. Both crystallize in the non-centrosymmetric space group $P2_1$. This phenomenon is rare for achiral molecules [35]. In this case, it is explained by the formation of wavy columns of molecules inverted to each other, forming only one of the two possible enantiomorphs (Fig. 1a). The molecules are not planar and the dihedral angle between the phenyl ring and the imidazo[1,5-a]pyridine core is 40° for both **4** and **5** (Fig. 1a and Fig. S2 for **4** and **5**, respectively). The columns are laterally associated to each other, forming layers of organic matter separated by planes of halogen substituents (Fig. 1b and Fig. S2b for **4** and **5**, respectively). Although the nitrogen atoms point toward the halogen atoms (Fig. S5), considering the measured angles (~144–145° for both), the corresponding distances (3.563 and 3.696 Å for 4 and 5, respectively) seem to be slightly longer with respect to those usually found for halogen bonding (d N···Br~3.4 Å and d N···I~3.5 Å) [34]. This feature was further evaluated by Hirshfeld surface (HS) analysis and by solid-state NMR spectroscopy (see below). Some differences can be observed moving from **4** and **5** to **7** and **9**. Indeed, **7** and **9** crystallize in a more common triclinic *P-1* space group. This is probably due to the formation of couples of inverted molecules, driven by dipolar interactions, generating also in this case stacked columns (Fig. 2a and Fig. S4 for **7** and **9**, respectively). This association is also strengthened by the presence of π–π stacking with a distance between central parallel aromatic cores of 3.5 Å [36]. In the columns, the halogen substituents point in opposite directions, forming alternating halogens and organic core layers (Fig. 2b and Fig. S4c for **7** and **9**, respectively). This disposition is quite different compared to the previous columnar one (compare Fig. 1a with Fig. 2a):

3-substituted imidazo[1,5-a]pyridines are disposed in non-parallel planes and the dominant interaction is a C–H···π contact between frontal aromatic rings, while in the case of 1,3-disubstituted imidazo[1,5-a]pyridines the central skeleton is on parallel planes and the dominant interaction is the π–π stacking between them (see HS analysis below). Since the pyridinic nitrogen in **9** does not participate to any strong directional interaction and the pyridyl does not significantly change the packing in comparison to the phenyl group, the resulting crystals of **7** and **9** are isomorphous. Finally, it is interesting to consider the effect of the presence/absence of a halide substituent in the molecular framework. Comparing the crystal packing of **7** to that of **6** (previously reported [7]) it is clear that, although there is no contribution from halogen bonds, the different polarity of the molecule changes the disposition of the molecular entities, leading to the formation of columns of inverted molecules as opposed to layers of parallel stacked molecules.

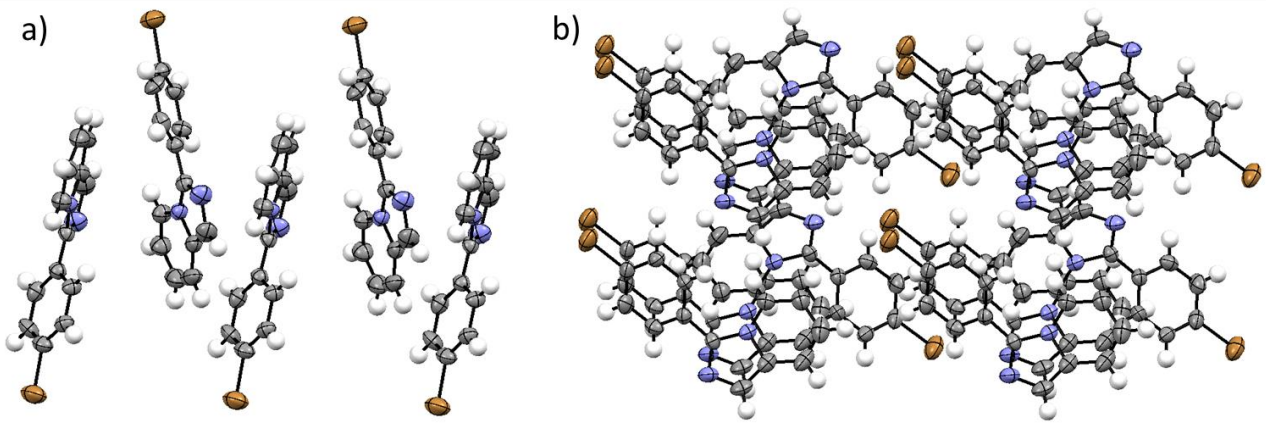

Fig. 1. Columns of inverted molecules (a) and associations of columns (b) in the crystal structure of **4**.

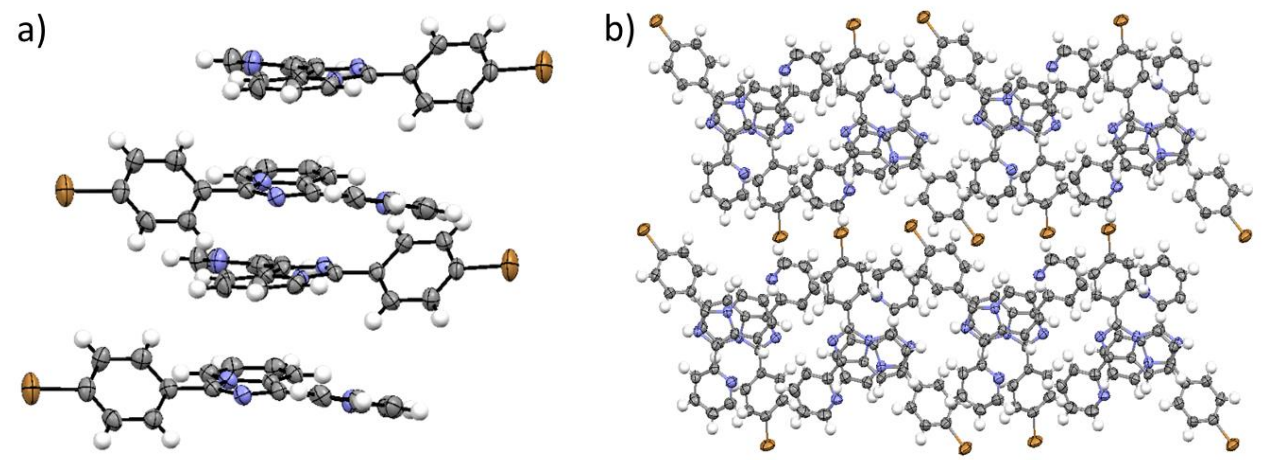

Fig. 2. Column of parallel molecules (a) and layers (b) in the crystal packing of **7**.

2.3 Hirshfeld surface analysis

HS analysis is a powerful tool for analysing intermolecular interactions in a more global manner compared to the usual "length and angles between atomic centres" point of view [37]. It highlights a surface that includes the region of the space containing most of the electron density of a single molecule. The use of instruments, such as topological derivatives and fingerprints, makes it possible to consider and observe subtle effects and very weak contacts [38]. By considering the results obtained in the case of **4**, in relation to the results obtained for **7**, it is possible to observe the

inversion of the role of C–H···π and π···π contacts. The first interaction is very strong and pervasive in both cases, as evident for the percentage of the covering of HS presented in Fig. 3b and Fig. 4b. However, for **4** its effect is spread all around the molecular structure (Fig. 3d), preventing the formation of π···π contacts. This situation is inverted in the case of **7**, in which the C–H···π contact is focused on the pyridyl group (the big red hollow on the shape index representation in Fig. 4d) while the central imidazo[1,5-a]pyridine core is free to participate to π···π interaction (demonstrated by the typical blue and red triangles in Fig. 4a). This inversion is explained by the difference in the conformation of the columns: products **4** and **5** show columns formed by non-parallel molecules, while **7** and **9** display columns of parallel molecules. However, despite the crystallographic (see above) and solid-state NMR (see below) analyses rule out the presence of halogen bond, in the case of **4** and **5** a weak contact region is present in the axis between X and N, using the Hirshfeld surface model [39]. The structures of **5** and **9** were not analysed due to their very strong similarity to **4** and **7** respectively, as reported in the previous section.

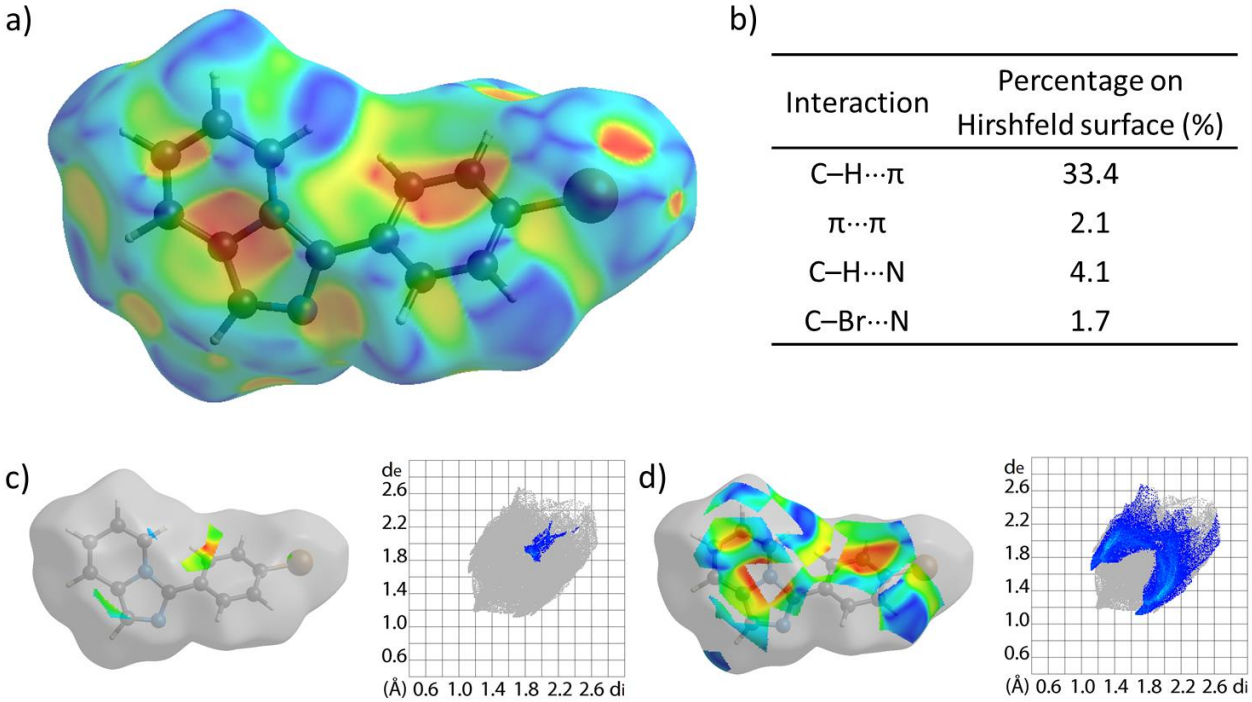

Fig. 3. (a) Representation of Shape Index on the Hirshfeld surface, (b) percentage of interaction components, (c) representation of π···π components and (d) representation of C–H···π components derived by the crystal structure of **4**.

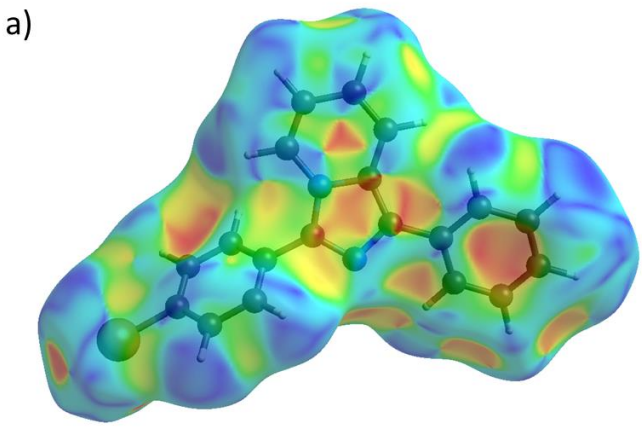

b)

Interaction	Percentage on Hirshfeld surface (%)
C–H···π	28.7
π···π	7.0
C–H···N	4.1
C–Br···N	0
C–Br···Br	0

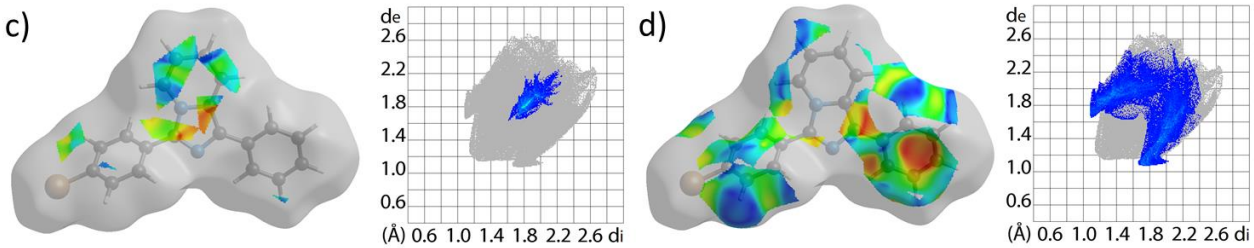

Fig. 4. (a) Representation of Shape Index on the Hirshfeld surface, (b) percentage of interaction components, (c) representation of π···π components and (d) representation of C–H···π components derived by the crystal structure of **7**.

2.4 Solid-state NMR

The presence of halogen bond interactions in compounds **3**–**5** was also investigated by means of solid-state NMR spectroscopy. Indeed, solid-state NMR is a powerful tool for assessing the occurrence of the halogen bond [40], offering information from chemical shift, quadrupolar coupling, dipolar coupling, and J-coupling [41–50]. Direct observation of the halogen bond donor has been limited to the study of ^{35}Cl due to the broad spectral widths associated with the heavier halogens which results in impractically broad peaks [49]. An effective option is a combination of pure Nuclear Quadrupolar Resonance (NQR) and nutation NQR which proved to be sensitive to small changes in the halogen bond geometry and allowed for the discrimination of crystallographically inequivalent halogen bonds [51]. Notably, solid-state NMR experiments on ^{13}C, ^{15}N, ^{31}P, or ^{77}Se have been used at natural isotopic abundance to evaluate geometrical features of the halogen bond [45,52,53]. In particular, solid-state ^{15}N chemical shifts of aromatic nitrogen atoms generally decrease upon halogen bond formation accordingly to the normalized contact. This proved that the ^{15}N isotropic chemical shifts are diagnostic of the geometry of the halogen bond, and their change upon halogen bond occurrence is generally greater than the change of ^{13}C chemical shifts providing an even better probe.

The ^{15}N cross-polarization magic angle spinning (CPMAS) spectra of samples **3**–**5** are reported in Fig. 5 in comparison with that of **1**. All spectra are characterized by two resonances at ca. 188 and 275 ppm attributed to the N(4) and N(1), respectively. In the presence of halogen bond, we expect a significant low-frequency shift of the signal at 275 ppm [52]. As no changes are observed for all compounds, the solid-state NMR analysis agrees with the lack of halogen bond in samples **3**–**5**, as already pointed out by the unfavourable geometry observed by single crystal X-ray diffraction.

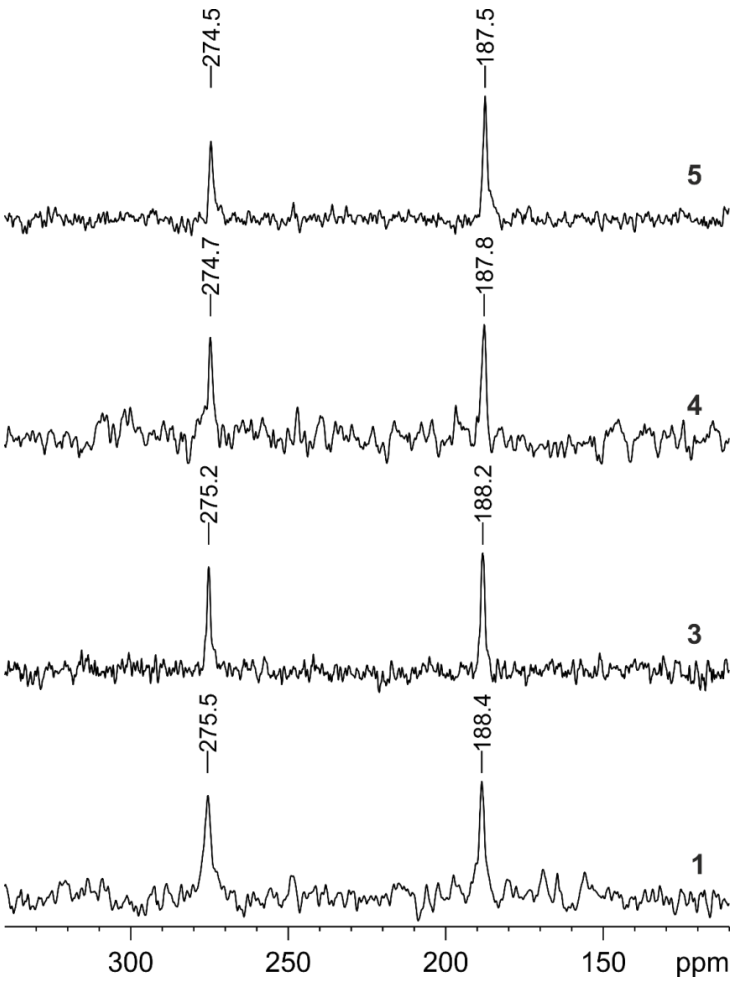

Fig. 5. ^{15}N (40.56 MHz) CPMAS spectra of samples **1**, **3**, **4**, and **5** acquired at 9 kHz.

2.5 Optical characterization

The imidazo[1,5-a]pyridine fluorogenic skeleton has been applied in a variety of technological applications such as organic thin-layer field effect transistors (OFETs), organic light-emitting diodes (OLEDs), downshifting technology, due to their large Stokes shift, intense UV absorption and remarkable quantum yield.

The UV–Vis absorption spectra of **1**–**9** in chloroform solution are shown in Fig. 6 and selected photophysical properties are reported in Table 1. The main absorption peaks for compounds **1**–**9** fall between 270 nm and 340 nm, with almost no absorption beyond 455 nm. Compounds **1**–**5** show a single maximum at about 320 nm, on the contrary **6**–**9** present two main bands, one in the 290–310 nm range and a second one centred at 320 or 340 nm.

The introduction of the halogen atom on the 3-phenylimidazo[1,5-a]pyridine (**1**) causes a red shift in the absorption spectra (about 15 nm, compounds **2**–**5**), on the contrary the introduction of the halogen in the same position on compounds **6** and **8** does not cause any noticeable shift in the absorption maxima (see compounds **7** and **9**).

In general, the absorption between 360 nm and 430 nm significantly increases going from compound **1**–**5** to compounds **6**–**9**, as a clear consequence of the extension of the conjugation due to insertion in position **3** of a phenyl or pyridyl substituent.

All the molecules, dissolved in chloroform solutions, under UV excitation display an intense fluorescence emission centred in the 450–480 nm range (Fig. 7). The introduction of different

halogen atoms on the phenyl moiety in position **3** has little influence on the emission maximum. On the other hand, the insertion of a pendant group in position 1 has a bathochromic effect, as previously reported in the literature [16,27,54]; in particular the substitution of a benzene ring with a pyridine one has a stronger effect on the emission spectra.

More noticeably, the chemical nature of the halogenated substituent in position 3 has a strong influence on the quantum yield of the compounds. Indeed we were able to tune the quantum yields in solution from 0.5% to 21.4% (Table 1) for the 3-phenylimidazo[1,5-a]pyridines (**1**–**9**). It is fascinating to note that the introduction of different halogens on the 3-phenyimidazo[1,5-a]pyridines (**1**–**5**) greatly and proportionally decrease the quantum yield and the lifetime along the halogen series. In particular, the radiative rate constant (kr) is the same for all the 5 molecules of the series (**1**–**5**) while the non-radiative rate constant (knr) dramatically increases in the case of the brominated (**4**) and iodinated (**5**) molecules, as a consequence of the increased spin–orbit coupling that favours the intersystem crossing to triplet states.

The same effect is observed on the 1-substituted imidazo[1,5-a]pyridine structure with quantum yield changing from 14.6% to 5.2% (**6** and **7**) or from 21.4% to 7.8% (**8** and **9**). In other words, the modification of the halogen on the imidazo[1,5-a]pyridine triplicates the optical performance in terms of quantum yield and lifetime. Moreover, moving from the 3-phenylimidazo[1,5-a]pyridine skeleton (**1**–**5**) to the 1,3-diphenylimidazo[1,5-a]pyridine skeleton (**6** and **7**), to the 3-phenyl-1-(pyridin-2-yl)imidazo[1,5-a]pyridine skeleton (**8** and **9**), allows obtaining a remarkable improvement in terms of quantum yield and lifetime, due to the increase of k_r and the concomitant decrease of k_{nr}.

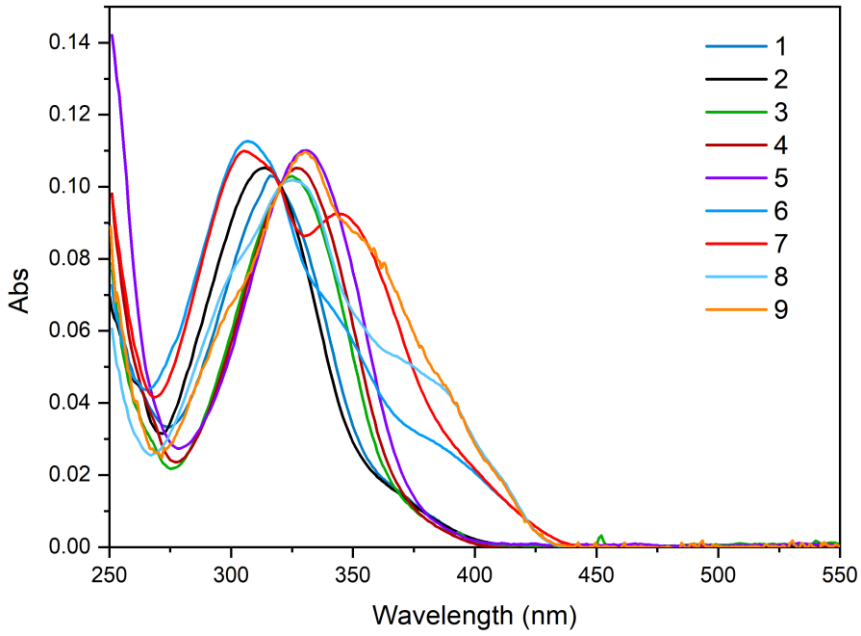

Fig. 6. Electronic absorption spectra of compounds **1**–**9** recorded in chloroform solution.

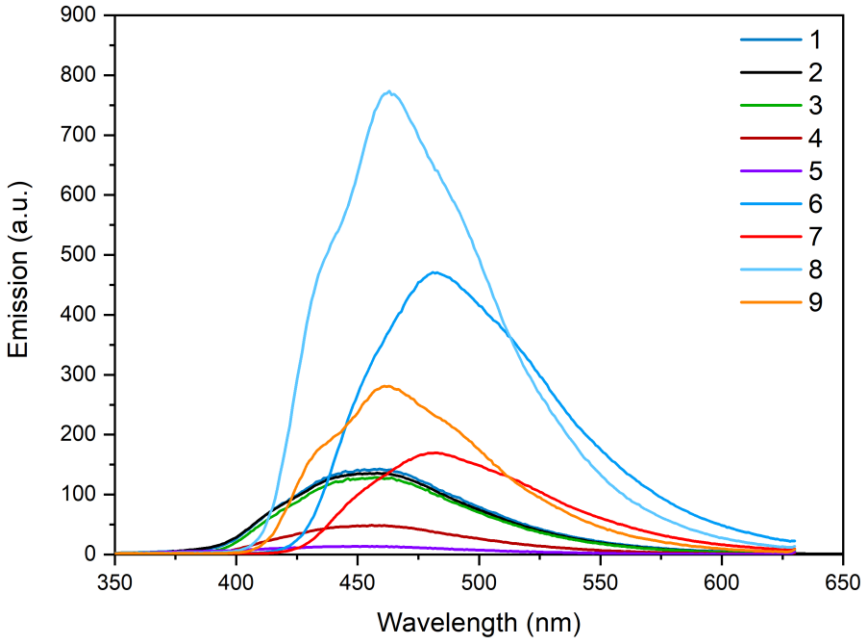

Fig 7. Electronic emission spectra of compounds **1**–**9** recorded in chloroform solution.

Table 1. Selected photophysical properties of compounds **1**–**9** in chloroform.

Compound	λ_{abs} (nm)	λ_{em} (nm)	Stokes Shift (nm)	φ (%)	τ (ns)	k_r (10^9 s^{-1})	k_{nr} (10^9 s^{-1})
1	317	456	139	4.4	1.8	0.024	0.53
2[a]	312	465	153	4.2	1.7	0.025	0.56
3	325	457	132	4.2	1.8	0.023	0.53
4	327	457	130	1.5	0.7	0.022	1.43
5	332	451	120	0.5	0.3	0.019	3.83
6	306 332sh 380sh	482	176	14.6	4.2	0.034	0.20
7	305 343sh	482	177	5.2	1.4	0.037	0.67
8	325 380sh	462	137	21.4	3.1	0.070	0.26
9	330 360sh	462	132	7.8	1.1	0.074	0.88

$k_r = \varphi/\tau$ and $k_{nr} = (1-\varphi)/\tau$

3. Materials and methods

3.1 Materials and techniques

All solvents and raw materials were used as received from commercial suppliers (Sigma-Aldrich and Alfa Aesar) without further purification. TLC was performed on Fluka silica gel TLC-PET foils GF 254, particle size 25 nm, medium pore diameter 60 Å. Column chromatography was performed on Sigma-Aldrich silica gel 60 (70-230 mesh ASTM).

^{1}H and ^{13}C solution NMR spectra were recorded on a JEOL ECP 400 FT-NMR spectrometer, operating at 399.8 and 100.5 MHz for ^{1}H and ^{13}C nuclei, respectively. Chemical shifts are reported relative to TMS (δ = 0) and referenced against solvent residual peaks. The following abbreviations are used: s (singlet), d (doublet), t (triplet), dd (doublet of doublets), m (multiplet). Solid-state NMR

spectra were acquired with a Bruker Avance II 400 Ultra Shield spectrometer, operating at 400.2 and 40.6 MHz for ^{1}H and ^{15}N nuclei, respectively. Powder samples were packed into cylindrical zirconia rotors with 4 mm o.d. and 80 μL volume and spun at 9 kHz. ^{15}N CPMAS spectra were acquired using a ramp cross-polarization pulse sequence with a 90° ^{1}H pulse of 3.60 μs, a contact time of 4 ms, optimized recycle delays of 21–75 s, a number of scans in the range 1000-7000, depending on the sample. For every spectrum, a two-pulse phase modulation (TPPM) decoupling scheme was used, with a radiofrequence field of 69.4 kHz. The ^{15}N chemical shift scale was calibrated through the signal of external standard glycine (at 33.4 ppm with reference to NH_3).
Mass spectra were recorded on a Thermo-Finnigan Advantage Max Ion Trap Spectrometer equipped with an electrospray ion source (ESI) in positive and negative ion acquiring mode.
Elemental composition was determined using a Thermo FlashEA 1112 CHNS–O analyser. Two replicas were performed and values were presented as % mass mean value.
FT-IR spectra were recorded on a Spectrum Two FT-IR Spectrometer (PerkinElmer) using ATR.
UV-Vis absorption spectra were recorded on a Cary60 spectrometer. Photoemission spectra, luminescence lifetimes and quantum yields were acquired with a HORIBA Jobin Yvon IBH Fluorolog-TCSPC spectrofluorometer, equipped with a Quanta-φ integrating sphere. The spectral response was corrected for the spectral sensitivity of the photomultiplier. Luminescence lifetimes were determined by time-correlated single-photon counting; excitation was achieved with nanosecond pulses generated by NanoLED pulsed diodes. Emission-decay data were collected in 2048 channels to 10000 counts in the peak channel and analysed with the software DAS6 (TCSPC decay-analysis software).
The single-crystal data were collected with a Gemini R Ultra diffractometer with graphite-monochromated Mo-*K*α radiation (λ = 0.71073) for products **4**, **5**, **7** and **9** by the ω-scan method. The cell parameters were retrieved with the CrysAlisPro software,[55] and the same program was used to perform data reduction and to apply Lorenz and polarization corrections. Scaling and absorption corrections were applied through the CrysAlisPro multiscan technique. All the structure has been solved with direct methods by using SHELXS-14.[56] All the structure has been refined with full-matrix least-squares techniques on F^2 with SHELXL-14 [57] using the program Olex2.0[58] All non-hydrogen atoms were refined anisotropically. Hydrogen atoms were calculated and riding on the corresponding bonded atoms. Representation and analysis of Hirshfeld Surface and their fingerprints has been obtained with the program CrystalExplorer.[59] Bond lengths and angles are reported in Tables S2–S9 and the crystal data and refinement results can be found in Table S1. The graphics of the crystal structure has been generated using Mercury 3.9.[60] 1868686-1868689 CCDC CODEs contain the supplementary crystallographic data for **4**, **5**, **7** and **6**. The CIF files have been checked with the CheckCIF quality service provided by CSD database and no important errors or imperfections have been detected. These data can be obtained free of charge via http://www.ccdc.cam.ac. uk/conts/retrieving.html, or from the Cambridge Crystallographic Data Centre, 12 Union Road, Cambridge CB2 1EZ, UK; fax: (+44) 1223-336-033; or e-mail: deposit@ccdc.cam.ac.uk.

3.2 Syntheses

Compounds **1**–**4** have been previously reported (**1** [31], **2** [28], **3** [61], **4** [62]) and were prepared with a slight modification of a previously published procedure [31]. Compounds **6**–**8** were

synthesized as previously reported (**6** [7], **7** [33], **8** [15,29]). The compounds **5** and **9** are new and never reported in the literature.

3.2.1 3-phenylimidazo[1,5-*a*]pyridine (**1**)

A microwave vial was charged with a solution of 2-picolylamine (0.175 g, 1.62 mmol) in *n*-butyl acetate (2.5 mL), T3P (propylphosphonic anhydride solution, ≥ 50 wt. % in ethyl acetate, 2.5 mL) and benzoic acid (0.235 g, 1.92 mmol). The vial was sealed and the resulting mixture was heated at 160°C by microwave for 45 min with stirring. The reaction mixture was cooled to room temperature and the n-butyl acetate distilled under vacuum. The obtained solid was dissolved in a saturated aqueous solution of Na_2CO_3 and the mixture extracted with CH_2Cl_2 (3 x 5 mL). The organic layer was separated, dried and the solvent evaporated under vacuum. The resulting solid was washed several times with diethyl ether and dried under vacuum obtaining the product as a yellow powder (yields 95%, 0.30 g), melting point 107-109 °C. ^{1}H NMR (400 MHz, $CDCl_3$): δ/ppm 8.27 (d, J = 7.2 Hz, 1H), 7.79 (d, J = 7.7 Hz, 2H), 7.57–7.42 (m, 5H), 6.74 (dd, J = 9.1, 6.4 Hz, 1H), 6.56 (t, J = 6.8 Hz, 1H), ^{13}C NMR (50 MHz, $CDCl_3$): δ/ppm 138.3, 131.7, 130.4, 129.0, 128.7, 128.0, 121.5, 120.7,118.9, 118.8, 113.1. FT-IR spectra (ATR) see Figure S6 (Supplementary data). MS (ESI) m/z calculated for $C_{13}H_{11}N_2$ ($[M+H]^+$): 195.09; found: 195.15. Elemental analysis: molecular formula $C_{13}H_{10}N_2$ requires C, 80.4; H, 5.2; N, 14.4%; found: C, 80.0; H, 5.2; N, 14.3%.

3.2.2 3-(4-chlorophenyl)imidazo[1,5-*a*]pyridine (**3**)

A microwave vial was charged with a solution of 2-picolylamine (0.166 g, 1.54 mmol) in *n*-butyl acetate (3.0 mL), T3P (propylphosphonic anhydride solution, ≥ 50 wt. % in ethyl acetate, 2.5 mL) and 4-chlorobenzoic acid (0.299 g, 1.91 mmol). The vial was sealed and the resulting mixture was heated at 160°C by microwave for 45 min with stirring. The reaction mixture was cooled to room temperature and the n-butyl acetate distilled under vacuum. The obtained solid was dissolved in a saturated aqueous solution of Na_2CO_3 and the mixture extracted with CH_2Cl_2 (3 x 5 mL). The organic layer was separated, dried and the solvent evaporated under vacuum. The resulting solid was washed several times with diethyl ether and dried under vacuum obtaining the product as a yellow powder (yields 92%, 0.32 g), melting point 99-101 °C. ^{1}H NMR (400 MHz, $CDCl_3$): δ/ppm 8.20 (d, J = 7.2 Hz, 1H), 7.74 (d, J = 7.4 Hz, 2H), 7.56 (s, 1H), 7.48 (d, J = 8.3 Hz, 3H), 6.80–6.70 (m, 1H), 6.57 (t, J = 6.8 Hz, 1H); ^{13}C NMR (100 MHz, $CDCl_3$) δ/ppm 137.1, 134.4, 131.8, 129.3, 129.1, 128.9, 121.2, 120.9, 119.0, 118.9, 113.4. FT-IR spectra (ATR) see Figure S6 (Supplementary data). MS (ESI) m/z calculated for $C_{13}H_{10}ClN_2$ ($[M+H]^+$): 229.05; found: 229.12. Elemental analysis: molecular formula $C_{13}H_9ClN_2$ requires C, 68.3; H, 4.0; N, 12.3%; found: C, 68.0; H, 4.0; N, 12.2%.

3.2.3 3-(4-bromophenyl)imidazo[1,5-*a*]pyridine (**4**)

A microwave vial was charged with a solution of 2-picolylamine (0.166 g, 1.54 mmol) in *n*-butyl acetate (3.0 mL), T3P (propylphosphonic anhydride solution, ≥ 50 wt. % in ethyl acetate, 2.5 mL) and 4-bromobenzoic acid (0.383 g, 1.91 mmol). The vial was sealed and the resulting mixture was heated at 160°C by microwave for 45 min with stirring. The reaction mixture was cooled to room temperature and the n-butyl acetate distilled under vacuum. The obtained solid was dissolved in a saturated aqueous solution of Na_2CO_3 and the mixture extracted with CH_2Cl_2 (3 x 5 mL). The organic layer was separated, dried and the solvent evaporated under vacuum. The formed solid was washed several times with diethyl ether and dried under vacuum obtaining the product as a yellow powder (yields 95%, 0.40 g), melting point 105-106 °C. ^{1}H NMR (400 MHz, $CDCl_3$): δ/ppm 8.20 (d, J = 7.1 Hz, 1H), 7.67 (q, J = 8.0 Hz, 4H), 7.56 (s, 1H), 7.50 (d, J = 9.1 Hz, 1H), 6.77 (dd, J = 9.1,

6.4 Hz, 1H), 6.58 (dd, J = 7.2, 6.4 Hz, 1H). ^{13}C NMR (100 MHz, $CDCl_3$): δ/ppm 137.1, 132.3, 131.9, 129.5, 129.2, 122.7, 121.3, 120.8, 119.3, 119.1, 113.8. FT-IR spectra (ATR) see Figure S6 (Supplementary data). MS (ESI) m/z calculated for $C_{13}H_{10}BrN_2$ ($[M+H]^+$): 273.00; found: 273.11. $C_{13}H_9BrN_2$ requires C, 57.2; H, 3.3; N, 10.3%; found: C, 56.8; H, 3.4; N, 10.2%.

3.2.4 3-(4-iodophenyl)imidazo[1,5-*a*]pyridine (**5**)

A microwave vial was charged with a solution of 2-methylaminopyridine (0.148 g, 1.37 mmol) in *n*-butyl acetate (2.5 mL), T3P (propylphosphonic anhydride solution, ≥ 50 wt. % in ethyl acetate, 2.5 mL) and 4-iodobenzoic acid (0.440 g, 1.78 mmol). The vial was sealed and the resulting mixture was heated at 160°C by microwave for 45 min with stirring. The reaction mixture was cooled to room temperature and the n-butyl acetate distilled under vacuum. The obtained solid was dissolved in a saturated aqueous solution of Na_2CO_3 and the mixture extracted with CH_2Cl_2 (3 x 5 mL). The organic layer was separated, dried and the solvent evaporated under vacuum. The formed solid was washed several times with diethyl ether and dried under vacuum obtaining the product as a yellow powder (yield: 92%, 0.40 g), melting point 120-122 °C. ^{1}H NMR (400 MHz, $CDCl_3$): δ/ppm 8.20 (d, J = 7.2 Hz, 1H), 7.85 (d, J = 8.2 Hz, 2H), 7.54 (m, 3H), 7.49 (d, J = 9.1 Hz, 1H), 6.74 (dd, J = 9.1, 6.4 Hz, 1H), 6.59 (t, J = 7.2 Hz, 1H). ^{13}C NMR (100 MHz, $CDCl_3$): δ/ppm 138.2, 137.3, 132.0, 130.0, 129.5, 121.3, 121.1, 119.1, 119.0, 113.6, 94.3. FT-IR spectra (ATR) see Figure S6 (Supplementary data). MS (ESI) m/z calculated for $C_{13}H_{10}IN_2$ ($[M+H]^+$): 320.99; found: 321.08. Elemental analysis: molecular formula $C_{13}H_9IN_2$ requires C, 48.8; H, 2.8; N, 8.8%; found: C, 48.5; H, 2.9; N, 8.7%.

3.2.5 3-(4-bromophenyl)-1-(pyridin-2-yl)imidazo[1,5-*a*]pyridine (**9**)

A microwave vial was charged with a solution of phenyl(pyridin-2-yl)methanone (0.800 g, 4.37 mmol), 4-iodobenzaldehyde (6.55 mmol), and ammonium acetate (1.704 g, 21.85 mmol) in glacial acetic acid (13 mL). The vial was sealed and the resulting mixture was heated at 180°C by microwave for 50 min with stirring. The reaction mixture was cooled to room temperature and the acetic acid was removed by evaporation under reduced pressure. The obtained solid was dissolved in a saturated aqueous solution of Na_2CO_3 and the mixture extracted with CH_2Cl_2 (3 x 5 mL). The organic layer was separated, dried and the solvent evaporated under vacuum. The obtained crude product was purified via column chromatography on silica gel (CH_2Cl_2/CH_3OH 98:2), obtaining the product as a yellow powder (yield: 71%, 1.08 g). Melting point 152-154 °C. ^{1}H NMR (400 MHz, $CDCl_3$): δ/ppm 8.72 (d, J = 9.2 Hz, 1H), 8.64 (d, J = 5.0 Hz, 1H), 8.22 (dd, J = 7.6, 5.0 Hz, 2H), 7.71 (m, 5H), 7.12 (dd, J = 7.5, 4.9 Hz, 1H), 6.95 (dd, J = 9.3, 7.4 Hz, 1H), 6.70 (t, J = 6.2 Hz, 1H), ^{13}C NMR (100 MHz, $CDCl_3$): δ/ppm 154.8, 149.0, 137.1, 136.6, 132.4, 130.6, 129.9, 129.2, 123.2, 122.1, 121.5, 121.4, 120.8, 120.2, 114.5, 77.5, 77.4, 77.2, 76.8. FT-IR spectra (ATR) see Figure S6 (Supplementary data). MS (ESI): m/z calculated for $C_{18}H_{13}BrN_3$ ($[M+H]^+$): 350.03; found: 350.06. Elemental analysis: molecular formula $C_{18}H_{12}BrN_3$ requires C, 61.7; H, 3.5; N, 12.0%; found: C, 61.4; H, 3.5; N, 11.9%.

4. Conclusions

A series of fluorescent substituted imidazo[1,5-a]pyridine derivatives was synthesized and structurally as well as electronically characterized. The luminescent imidazo[1,5-a]pyridine core was successfully substituted in position 3 with different halogens and in position 1 with phenyl or pyridyl pendant groups, deeply modifying the optical properties of this promising scaffold.

The structure of the obtained compounds was confirmed by ^{1}H NMR, ^{13}C NMR and Electrospray Ionization Mass Spectrometry. Single-crystal X-ray diffraction structures of **4**–**7** and **9** were analysed to investigate the presence of halogen bond and the effect of different substituents in the molecular framework on the crystal packing. The greatest difference is between products with or without the halide substituent, due to the different polarity. Indeed, no evidence of halogen bond formation was obtained, although the nitrogen atoms often point toward the halogen atoms. Hirshfeld surface analysis allowed to rationalize the contributions of C–H···π and π···π stacking in the different motifs obtained with 3-substituted or 1,3-disubstituted imidazo[1,5-a]pyridines, suggesting an inversion of their influence on the definition of the crystal packing.

Electronic absorption and emission spectra of the compounds were investigated in chloroform solutions. Our 1,3-substituted imidazo[1,5-a]pyridines show absorption maxima below 420 nm, with a respectable transparency in the visible range, and intense emissions at wavelengths in the 450–480 nm range. The introduction of different halogens on the phenyl in position 3 on imidazo[1,5-a]pyridine and the modification of the pendant group in position 1 strongly modify the optical properties. The absence of the pendant group in position 1 (compounds **1**–**5**) on the imidazo[1,5-a]pyridine nucleus causes a strong diminution of the quantum yield and a slight blue shift in the absorption spectra, in comparison to the other studied compounds (**6**–**9**). The noticeable increase of the emission quantum yield (up to three times) from 5.2% or 7.8% to 14.6% or 21.4% (for **7**, **9**, **6**, **8** respectively) evidences a strong dependence of the optical properties from the halogen substituent. Furthermore, for the first time the radiative and non-radiative deactivation constants were systematically evaluated for the imidazo[1,5-a]pyridine scaffold, highlighting the dramatic effect of the halogen substituent and chemical structure on the fluorescence quantum yield and lifetime.

In summary, this work highlights how the chemical substitution in position 1 is fundamental to improve the optical properties of these fluorophores. Moreover, although halogenated derivatives suppress the optical properties of the imidazo[1,5-a]pyridine nucleus, they represent an essential class of intermediates for subsequent derivatizations, whose products show a complete recovery of the optical properties.

References

[1] J.A. Joule, K. Mills, Heterocyclic Chemistry, 4 edition, Wiley-Blackwell, Oxford, 2000.

[2] B.P. Fauber, A. Gobbi, K. Robarge, A. Zhou, A. Barnard, J. Cao, Y. Deng, C. Eidenschenk, C. Everett, A. Ganguli, J. Hawkins, A.R. Johnson, H. La, M. Norman, G. Salmon, S. Summerhill, W. Ouyang, W. Tang, H. Wong, Bioorg. Med. Chem. Lett. 25 (2015) 2907–2912.

[3] M.A. Ingersoll, A.S. Lyons, S. Muniyan, N. D'Cunha, T. Robinson, K. Hoelting, J.G. Dwyer, X.R. Bu, S.K. Batra, M.-F. Lin, PLOS ONE 10 (2015) e0131811.

[4] M. Roy, B.V.S.K. Chakravarthi, C. Jayabaskaran, A.A. Karande, A.R. Chakravarty, Dalton Trans. 40 (2011) 4855–4864.

[5] S. Fuse, T. Ohuchi, Y. Asawa, S. Sato, H. Nakamura, Bioorg. Med. Chem. Lett. 26 (2016) 5887–5890.

[6] S. Priyanga, T. Khamrang, M. Velusamy, S. Karthi, B. Ashokkumar, R. Mayilmurugan, Dalton Trans. 48 (2019) 1489–1503.

[7] G. Volpi, G. Magnano, I. Benesperi, D. Saccone, E. Priola, V. Gianotti, M. Milanesio, E. Conterosito, C. Barolo, G. Viscardi, Dyes Pigments 137 (2017) 152–164.

[8] G.A. Ardizzoia, S. Brenna, S. Durini, B. Therrien, Polyhedron 90 (2015) 214–220.

[9] G.A. Ardizzoia, S. Brenna, S. Durini, B. Therrien, M. Veronelli, Eur. J. Inorg. Chem. (2014) 4310–4319.

[10] G. Albrecht, J.M. Herr, M. Steinbach, H. Yanagi, R. Göttlich, D. Schlettwein, Dyes Pigments 158 (2018) 334–341.

[11] G. Albrecht, C. Geis, J.M. Herr, J. Ruhl, R. Göttlich, D. Schlettwein, Org. Electron. 65 (2019) 321–326.
[12] D.R. Mohbiya, N. Sekar, ChemistrySelect 3 (2018) 1635–1644.
[13] E. Fresta, G. Volpi, C. Garino, C. Barolo, R.D. Costa, Polyhedron 140 (2018) 129–137.
[14] M.D. Weber, C. Garino, G. Volpi, E. Casamassa, M. Milanesio, C. Barolo, R.D. Costa, Dalton Trans. 45 (2016) 8984–8993.
[15] L. Salassa, C. Garino, A. Albertino, G. Volpi, C. Nervi, R. Gobetto, K.I. Hardcastle, Organometallics 27 (2008) 1427–1435.
[16] F. Shibahara, E. Yamaguchi, A. Kitagawa, A. Imai, T. Murai, Tetrahedron 65 (2009) 5062–5073.
[17] F. Shibahara, R. Sugiura, E. Yamaguchi, A. Kitagawa, T. Murai, J. Org. Chem. 74 (2009) 3566–3568.
[18] H. Wang, W. Xu, Z. Wang, L. Yu, K. Xu, J. Org. Chem. 80 (2015) 2431–2435.
[19] H.T.H. Nguyen, O.T.K. Nguyen, T. Truong, N.T.S. Phan, Rsc Adv. 6 (2016) 36039–36049.
[20] A.P. Krapcho, J.R. Powell, Tetrahedron Lett. 27 (1986) 3713–3714.
[21] Y.Q. Ge, B.Q. Hao, G.Y. Duan, J.W. Wang, J. Lumin. 131 (2011) 1070–1076.
[22] F. Shibahara, A. Kitagawa, E. Yamaguchi, T. Murai, Org. Lett. 8 (2006) 5621–5624.
[23] G. Volpi, C. Magistris, C. Garino, Nat. Prod. Res. 32 (2018) 2304–2311.
[24] G. Volpi, C. Magistris, C. Garino, Educ. Chem. Eng. 24 (2018) 1–6.
[25] G. Schäfer, M. Ahmetovic, S. Abele, Org. Lett. 19 (2017) 6578–6581.
[26] D.O. Tverdiy, M.O. Chekanov, P.V. Savitskiy, A.R. Syniugin, S.M. Yarmoliuk, A.A. Fokin, Synth. Ger. 48 (2016) 4269–4277.
[27] E. Yamaguchi, F. Shibahara, T. Murai, J. Org. Chem. 76 (2011) 6146–6158.
[28] E. Yamaguchi, F. Shibahara, T. Murai, Chem. Lett. 40 (2011) 939–940.
[29] J. Wang, L. Dyers, R. Mason, P. Amoyaw, X. Bu, J. Org. Chem. 70 (2005) 2353–2356.
[30] G. Volpi, C. Garino, E. Conterosito, C. Barolo, R. Gobetto, G. Viscardi, Dyes Pigments 128 (2016) 96–100.
[31] J.M. Crawforth, M. Paoletti, Tetrahedron Lett. 50 (2009) 4916–4918.
[32] G. Volpi, C. Garino, E. Priola, E. Diana, R. Gobetto, R. Buscaino, G. Viscardi, C. Barolo, Dyes Pigments 143 (2017) 284–290.
[33] G. Volpi, B. Lace, C. Garino, E. Priola, E. Artuso, P. Cerreia Vioglio, C. Barolo, A. Fin, A. Genre, C. Prandi, Dyes Pigments 157 (2018) 298–304.
[34] G. Cavallo, P. Metrangolo, R. Milani, T. Pilati, A. Priimagi, G. Resnati, G. Terraneo, Chem. Rev. 116 (2016) 2478–2601.
[35] E. Pidcock, Chem. Commun. 0 (2005) 3457–3459.
[36] C. Janiak, J. Chem. Soc. Dalton Trans. 0 (2000) 3885–3896.
[37] J.J. McKinnon, M.A. Spackman, A.S. Mitchell, Acta Crystallogr. Sect. B-Struct. Sci. 60 (2004) 627–668.
[38] J.J. McKinnon, D. Jayatilaka, M.A. Spackman, Chem. Commun. (2007) 3814–3816.
[39] M.A. Spackman, P.G. Byrom, Chem. Phys. Lett. 267 (1997) 215–220.
[40] P.C. Vioglio, M.R. Chierotti, R. Gobetto, CrystEngComm 18 (2016) 9173–9184.
[41] M. Baldrighi, G. Cavallo, M.R. Chierotti, R. Gobetto, P. Metrangolo, T. Pilati, G. Resnati, G. Terraneo, Mol. Pharm. 10 (2013) 1760–1772.
[42] M. Baldrighi, D. Bartesaghi, G. Cavallo, M.R. Chierotti, R. Gobetto, P. Metrangolo, T. Pilati, G. Resnati, G. Terraneo, Crystengcomm 16 (2014) 5897–5904.
[43] C.M. Widdifield, G. Cavallo, G.A. Facey, T. Pilati, J. Lin, P. Metrangolo, G. Resnati, D.L. Bryce, Chem.- Eur. J. 19 (2013) 11949–11962.
[44] J. Viger-Gravel, S. Leclerc, I. Korobkov, D.L. Bryce, Crystengcomm 15 (2013) 3168–3177.
[45] J. Viger-Gravel, J.E. Meyer, I. Korobkov, D.L. Bryce, Crystengcomm 16 (2014) 7285–7297.
[46] J. Viger-Gravel, S. Leclerc, I. Korobkov, D.L. Bryce, J. Am. Chem. Soc. 136 (2014) 6929–6942.
[47] M. Weingarth, N. Raouafi, B. Jouvelet, L. Duma, G. Bodenhausen, K. Boujlel, B. Schoellhorn, P. Tekely, Chem. Commun. (2008) 5981–5983.
[48] Y. Xu, J. Viger-Gravel, I. Korobkov, D.L. Bryce, J. Phys. Chem. C 119 (2015) 27104–27117.
[49] P.M.J. Szell, D.L. Bryce, J. Phys. Chem. C 120 (2016) 11121–11130.
[50] R.J. Attrell, C.M. Widdifield, I. Korobkov, D.L. Bryce, Cryst. Growth Des. 12 (2012) 1641–1653.
[51] P.C. Vioglio, P.M.J. Szell, M.R. Chierotti, R. Gobetto, D.L. Bryce, Chem. Sci. 9 (2018) 4555–4561.
[52] P. Cerreia Vioglio, L. Catalano, V. Vasylyeva, C. Nervi, M.R. Chierotti, G. Resnati, R. Gobetto, P. Metrangolo, Chem.- Eur. J. 22 (2016) 16817–16826.

[53] J. Viger-Gravel, I. Korobkov, D.L. Bryce, Cryst. Growth Des. 11 (2011) 4984–4995.
[54] F. Shibahara, E. Yamaguchi, T. Murai, Chem. Commun. 46 (2010) 2471–2473.
[55] CrysAlisPro, Rigaku Oxford Diffraction, Oxford, U.K., 2015.
[56] G.M. Sheldrick, Acta Crystallogr. Sect. A 64 (2008) 112–122.
[57] G.M. Sheldrick, Acta Crystallogr. Sect. C Struct. Chem. 71 (2015) 3–8.
[58] O.V. Dolomanov, L.J. Bourhis, R.J. Gildea, J.A.K. Howard, H. Puschmann, J. Appl. Crystallogr. 42 (2009) 339–341.
[59] M.A. Spackman, D. Jayatilaka, Crystengcomm 11 (2009) 19–32.
[60] C.F. Macrae, P.R. Edgington, P. McCabe, E. Pidcock, G.P. Shields, R. Taylor, M. Towler, J. van De Streek, J. Appl. Crystallogr. 39 (2006) 453–457.
[61] V.S. Arvapalli, G. Chen, S. Kosarev, M.E. Tan, D. Xie, L. Yet, Tetrahedron Lett. 51 (2010) 284–286.
[62] M. Li, Y. Xie, Y. Ye, Y. Zou, H. Jiang, W. Zeng, Org. Lett. 16 (2014) 6232–6235.